INSTITUTE OF PHYSICS PUBLISHING CLASSICAL AND QUANTUM GRAVITY

Class. Quantum Grav. **23** (2006) S277–S285 doi:10.1088/0264-9381/23/8/S35

Measurement of the thermoelastic properties of crystalline Si fibres

M Alshourbagy[1,2], P Amico[3,4], L Bosi[3,4], G Cagnoli[5,6], E Campagna[6,7], F Cottone[3,8], A Dari[3,8], L Gammaitoni[3,4], M Lorenzini[6,9], G Losurdo[6], F Marchesoni[3,8], F Martelli[6,7], F Piergiovanni[6,7], M Punturo[3], A Toncelli[1,2], M Tonelli[1,2], F Travasso[3,4], F Vetrano[6,7] and H Vocca[3,4]

[1] Istituto Nazionale di Fisica Nucleare, Sez. di Pisa, Largo B Pontecorvo 3, 56127 Pisa, Italy
[2] Dipartimento di Fisica, Università di Pisa, Largo B Pontecorvo 3, 56127 Pisa, Italy
[3] Istituto Nazionale di Fisica Nucleare, Sez. di Perugia, Via A Pascoli 1, 06123 Perugia, Italy
[4] Dipartimento di Fisica, Università di Perugia, Via A Pascoli 1, 06123 Perugia, Italy
[5] Institute for Gravitational Research, Department of Physics and Astronomy, University of Glasgow, G12 8QQ Glasgow, UK
[6] Istituto Nazionale di Fisica Nucleare, Sez. di Firenze, Via G Sansone 1, 50019 Sesto Fiorentino (FI), Italy
[7] Istituto di Fisica, Università di Urbino, Via S Chiara 27, 61029 Urbino, Italy
[8] Dipartimento di Fisica, Università di Camerino, Via Madonna delle Carceri 9, 62032 Camerino (MC), Italy
[9] Dipartimento di Astronomia e Scienze dello Spazio, Università di Firenze, Largo E Fermi 2, 50125 Firenze, Italy

E-mail: martelli@fi.infn.it

Received 6 September 2005, in final form 5 January 2006
Published 28 March 2006
Online at stacks.iop.org/CQG/23/S277

Abstract

In order to reduce the thermal noise in future interferometers for gravitational wave (GW) detectors, new suspension materials with low thermal noise are under investigation. Crystalline silicon seems to be a promising material mainly at low temperature. A new technology to produce crystalline silicon fibres has been realized. Measurements of mechanical and thermal properties of the fibres at room temperature have been performed. Preliminary measurements at low temperature are presented.

PACS numbers: 01.30.Cc, 04.80.Nn, 81.10.Fq, 81.40.Jj

(Some figures in this article are in colour only in the electronic version)

1. Introduction

In a range of frequency up to 100 Hz, the design sensitivity curve of advanced gravitational wave (GW) interferometric detectors is limited by thermal noise in the optics suspensions.

Materials with low loss angle values are necessary to reduce the thermal noise. New suspension materials are under investigation. Fused silica is a good material for room temperature interferometers [1–3] and the GEO600 detector has already adopted monolithic fused silica suspensions [4]. Crystalline silicon is also a very promising material [5, 6] for its mechanical and thermal properties mainly at cryogenic temperatures. At room temperature and at low temperature the silicon intrinsic loss angle is very low ($\simeq 10^{-8}$) [7–9], so the main contribution to dissipation is due to the thermoelastic effect. The thermoelastic loss angle for a cylindrical fibre of diameter d, specific heat per unit volume c_v and Young's modulus E is

$$\phi_{\rm th}(f) = \Delta \frac{f/f_p}{1 + (f/f_p)^2}, \tag{1}$$

where [10, 11]

$$\Delta = \frac{E\alpha^2 T}{c_v} \qquad f_p = 2.16 \frac{\kappa}{c_v d^2}. \tag{2}$$

The thermal expansion coefficient α of Si decreases with temperature until it vanishes at about 123 K, is negative down to about 17 K and almost zero below. So the thermoelastic dissipation decreases rapidly with temperature and becomes negligible, with respect to the structural loss, at around 120–130 K and under 20 K. The thermal conductivity κ is very high at room temperature and increases at low temperature down to 20 K [12–14]. Therefore, going down in temperature, the thermoelastic peak should move to higher frequencies and the heat extraction from the test mass is more efficient. For these reasons crystalline silicon is a good candidate for realizing cryogenic suspensions.

2. Silicon fibre production

Crystalline silicon fibres are grown in Pisa using the micro pulling down technique (μ-PD) [15]. The starting material is a melt of pure silicon. The melt is placed in vitreous carbon crucibles, heated with a radio frequency generator (see figure 2). The furnace's maximum operating temperature is around 2100 °C. A seed of crystalline silicon is inserted into the crucible orifice and pulled downward with a precise pulling mechanism. The melt passes through the nozzle and a new fibre is grown. The crystal growth rate is from 0.3 to 2 mm min^{-1}. An after heater placed under the crucible allows us to control the temperature gradient in the growing fibre. In that way, it is possible to adjust the position of the solid–liquid interface near the crucible tip. With a CCD camera, visual observation of the meniscus region of the solid–liquid interface and of the crystal growth is possible.

The furnace has been tested with several materials and about 15 crystalline silicon fibres have been grown with diameters ranging from 0.3 to 3 mm and lengths up to 310 mm.

Growth of long crystalline fibres is affected by vibrations which become especially intense at longer lengths [16]. In the first produced fibres some abrupt change in diameter was probably due to instabilities of the RF generator; anyway for most of their length the fibres show good regularity. The crystalline orientation of the fibres was determined using the Laue x-ray diffraction method: the inspected parts showed a single crystalline character, but the orientation changes along the fibre length at every point where the diameter is not stable.

As a result the fibres are not single crystals along all their length, but are composed of several single-crystal parts.

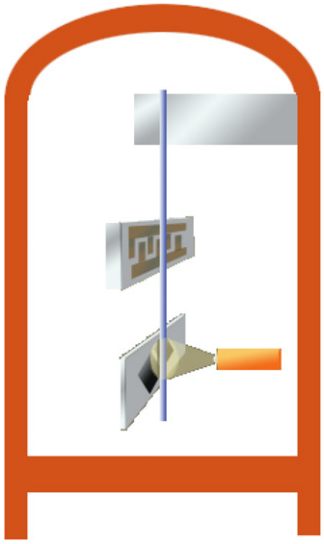

Figure 1. Simple diagram of the ring-down measurement setup. The fibre is clamped between two aluminium blocks (at the top) and it is excited by a high-gradient electric field produced by a set of comb electrodes (in the middle). The motion of the fibre is detected by an optical system known as shadow sensor. When the fibre is illuminated by a bright LED, the fibre casts a shadow on a pair of photodiodes. The transversal vibration of the fibre causes a differential photocurrent in the two photodiodes. The whole setup is kept in vacuum.

3. Measurement of thermoelastic properties

3.1. Loss angle measurement

Loss angle measurements are performed using a ring-down technique [2]. Because of the dielectric properties of Si, it is possible to induce the fibre resonance modes using a comb capacitor exciter driven by a high-voltage oscillating signal (see figure 1). The position of the fibre is measured using two side-by-side photodiodes and an IR-emitter forming a shadow sensor. The fibre is clamped at one end using two aluminium blocks, fixed to a massive rigid stand in order to minimize the recoil losses. The whole system is put in a vacuum chamber at a residual gas pressure of 10^{-5}–10^{-6} mbar. Air damping losses are reduced to a negligible level. The sensor output signal is processed by a digital lock-in amplifier in order to filter the signal and to lower the acquisition rate. Through the Hilbert transform of the filtered signal, the characteristic decay time τ of the ring down is extracted and the loss angle ϕ is calculated using

$$\phi = \frac{1}{\pi f \tau}, \tag{3}$$

f being the resonance frequency of the mode.

3.2. Modelling

The irregular profile of the fibres has been measured by a shadow-meter-based system. The fibre is rotated and moved along its axis across a laser beam. A photodiode detects the shadow of the fibre, while the laser light is sampled by a beam splitter and is focused on a second

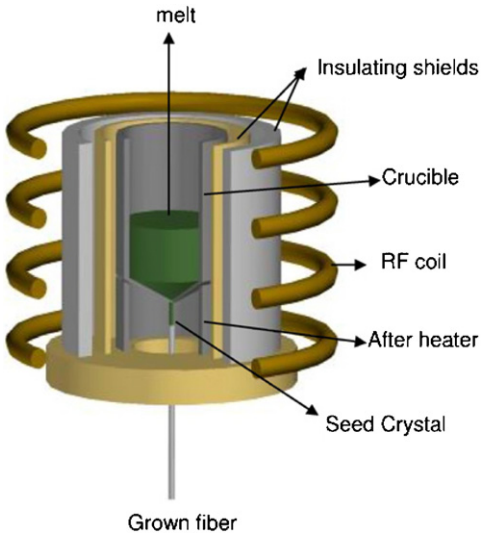

Figure 2. Schematic diagram for the μ-PD growth apparatus (hot zone part).

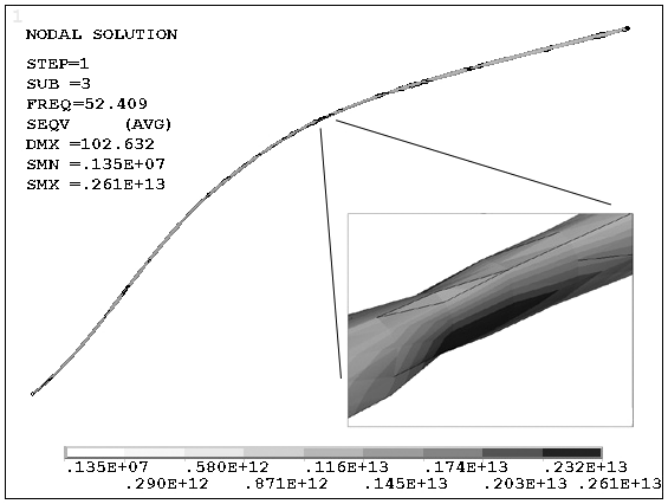

Figure 3. The simulated second mode of a 308 mm long fibre. In the enlarged box local stress distribution is also visible.

photodiode to get a reference signal. At a given point along the axis, for a given rotation angle, the diameter of the fibre is measured by the ratio between the signals of the two photodiodes. The system is calibrated with a series of well-known diameter wires. With the measured data, a finite element model of the fibre has been realized using FEM software (ANSYS). Figure 3 shows the second mode of a 308 mm fibre. Through this model, it is possible to extract the resonance mode frequencies of one-end clamped fibres.

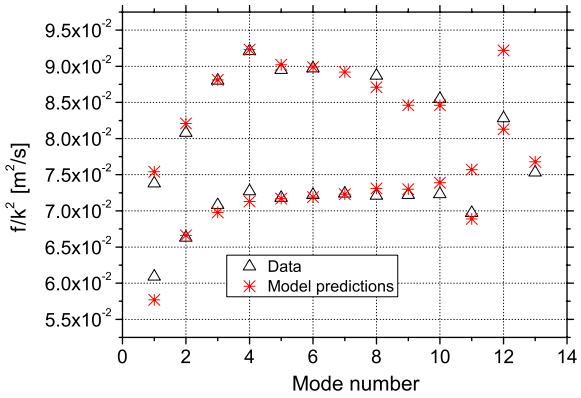

Figure 4. Values of f/k^2 for the 111.5 mm long fibre. The roughly elliptical section splits the curve into two branches. △, measurements; ⋆, prediction.

Table 1. Measured parameters for two crystalline Si fibres. At room temperature, $\alpha = 2.62 \times 10^{-6}$ K^{-1} and $\kappa = 148$ W m^{-1} K^{-1} [12].

L (mm)	E (GPa)	α (K^{-1})	κ (W m^{-1} K^{-1})	c
111.5 ± 0.5	150 ± 11	$(2.54 \pm 0.13) \times 10^{-6}$	146 ± 13	0.018 ± 0.002
308.0 ± 0.5	174 ± 12	$(2.56 \pm 0.11) \times 10^{-6}$	138 ± 11	–

3.3. Evaluation of Young's modulus

For an ideal cylindrical fibre, the ratio of the frequency f and the square wave number k^2 is a constant depending only on the geometry and Young's modulus. In contrast, for the produced fibres this ratio depends on the mode reflecting the geometric irregularities. In figure 4 are shown, for each mode, the values of f/k^2 as they come from the FEM and the measurements of a fibre. The best Young's modulus E has been evaluated matching the two sets as reported in table 1. The error comes mainly from the diameter uncertainty. The obtained values are close to what is expected for crystalline silicon.

4. Measurement results

Loss angle measurements have been performed on two crystalline silicon fibres whose lengths were, respectively, 308 mm and 111.5 mm, grown using a ⟨1 0 0⟩ oriented Si seed.

The results for the first fibre are compared in figure 5 with the thermoelastic model. Since the shape of the fibre is irregular, the predictions of the model are obtained assuming a cylindrical-shaped fibre with an 'effective' diameter given by the dispersion relation with the value of E measured through the FEM model, for each resonance mode. From the figure it is clear that an excess loss is present, probably due to contaminants on the fibre surface. Therefore, an etching process has been performed, removing the outer layer of the fibre and reducing the mean diameter to 574 μm. An isotropic etching can be obtained putting the fibre for 15–30 min at room temperature in a 75% HNO_3, 20% HF, 5% CH_3 COOH solution (HNA). In figure 6, the measured loss angles after etching are shown together with the modelled ones. The excess loss has been strongly reduced. The same measurements were performed on a second fibre (figure 7).

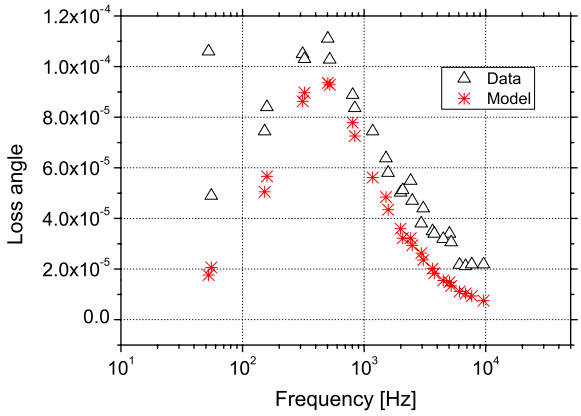

Figure 5. Measured loss angle of a 308 mm long fibre with an average diameter of 746 μm. $\triangle$, measurements; $\star$, prediction.

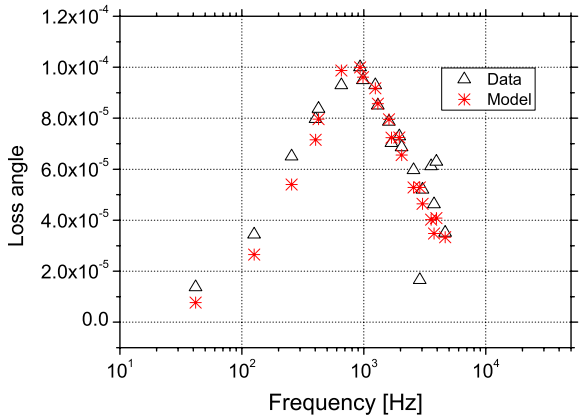

Figure 6. Measured loss angle and predicted thermoelastic loss for the same fibre as figure 5 after the HNA etching process. The diameter of the fibre is now 574 μm. $\triangle$, measurements; $\star$, prediction.

The shape of the thermoelastic peak allows us to fit the values of the thermal expansion coefficient α and the thermal conductivity κ. The height of the peak completely determines α, with the specific heat c_v taken from the literature [12]. The error comes mainly from the discrete sampling of the ϕ curve and is evaluated using the maximum and minimum slopes around the peak. Moreover, the thermal conductivity can be extracted from the peak frequency, since the characteristic time of heat flow is

$$\tau = \frac{1}{f_p} = F\frac{c_v d^2}{\kappa}, \tag{4}$$

where F is a factor taking into account the specific geometry of the fibre section ($F = 1/2.16$ for a cylindrical fibre) [10, 11]. For a roughly elliptical fibre section, the heat flow time is different along the two principal axes. This fact is accounted for by introducing a correction parameter c, so that $F = (1 \pm c)/2.16$. Therefore, it was possible to fit κ and c using the experimental values. The errors on the parameters were evaluated varying E and α within their errors. The results for α, κ and c are reported in table 1. The parameter c for the 308 mm fibre is compatible with zero, reflecting the almost circular shape of the fibre section.

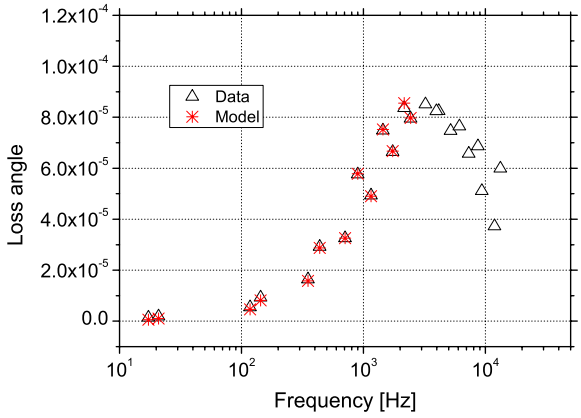

Figure 7. Measured loss angle and predicted thermoelastic loss for the 111.5 mm fibre after the HNA etching process. △, measurements; ⋆, prediction.

The modes above number 8 do not have a fixed oscillation plane and some of them are not pure bending modes. In these cases there is not a suitable model.

5. Measurement at low temperature

The 111.5 mm long fibre was measured also at low temperatures (down to 80 K) using a liquid nitrogen cryostat, while the 308 mm fibre was too long to be hosted inside the chamber. The fibre was kept in a copper clamp by means of a spring that should maintain the clamping pressure constant.

5.1. Young's modulus temperature dependence

To study the Young's modulus temperature dependence, three mode frequencies of the fibre have been tracked down to 80 K. At several temperatures, Young's modulus has been worked out according to

$$\frac{E(T) - E(291\,\mathrm{K})}{E(291\,\mathrm{K})} = \frac{1}{N}\sum_{1}^{N}\frac{f^2(T) - f^2(291\,\mathrm{K})}{f^2(291\,\mathrm{K})}, \tag{5}$$

where N is the number of considered modes. The results are shown in figure 8 together with four semi-empirical trends. Three curves are extrapolations at low temperature of the tabulated values of E [12] for each crystallographic orientation; the curve labelled as 'model fit' comes from the model described in [17, 18], valid in a wide temperature range

$$E(T) = E(0) - BT\,\mathrm{e}^{-\frac{T_0}{T}}, \tag{6}$$

where $E(0), B, T_0$ are constant parameters. This curve agrees with the experimental data for the parameter values reported in the figure, in good agreement with other measurements [18].

5.2. Loss angle measurements

The performed cryogenic measurements of loss angles reveal the presence of excess losses below 2 kHz, which are presumed to be mainly due to the clamp and to the recoil of the

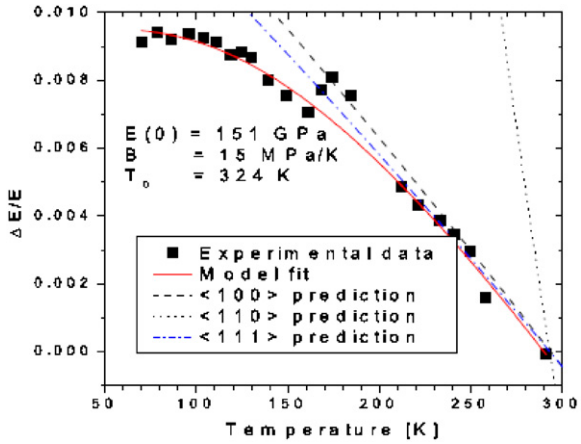

Figure 8. Relative Young's modulus variation versus T for the 111.5 mm fibre. The solid line is a fit to the model [17, 18]; the other curves are extrapolations at low T of the tabulated values of E [12], for each crystallographic orientation.

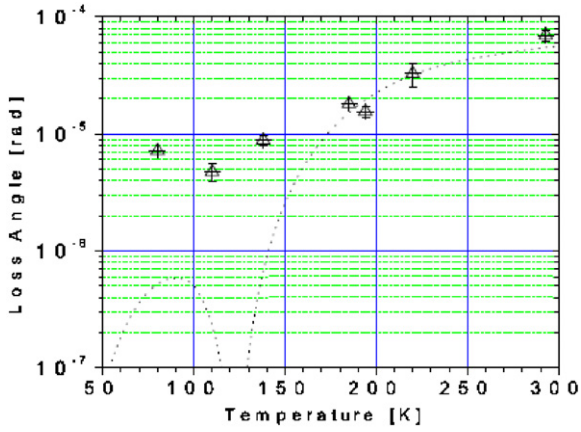

Figure 9. Temperature dependence of the measured loss angle for the 6680 Hz mode. The dotted line is the predicted thermoelastic contribution.

support. Therefore, in order to determine the temperature dependence of the loss angle, a mode with a frequency of 6680 Hz has been selected. Figure 9 shows the measured ϕ values; the dotted curve is the expected thermoelastic dissipation. Below 160 K the presence of a large excess loss is evident, whose origin is not well understood. This measurements can be compared with analogous ones on cantilever blades done by other groups [18]. Earlier works show that the expected losses for bulk silicon are of the order of 10^{-8} [7, 19, 20]. The observed behaviour can be justified by a dominating excess loss that will be investigated and possibly reduced in the near future.

6. Conclusions

In this paper, the results of the thermomechanical characterization of silicon fibres produced with the technique of μ-pulling have been presented. An accurate profiling of the samples

allowed precise measurement of Young's modulus and precise estimation of the thermoelastic effect. The results have shown that μ-pulling is a suitable technique for the production of silicon fibres as test samples, although some improvements are still needed to maintain the orientation of the crystal axis along the fibre length. A further study may investigate the possibility of using this technology for the production of suspension elements in future detectors. Loss measurements at room temperature and at low temperature have been performed showing that the etching of a few tens of micron is necessary to reduce the losses close to the thermoelastic limit. At low temperature, some unknown excess losses dominate at low frequency below 2 kHz. Above this frequency, the dependence of the measured loss on the temperature is consistent with results from other groups. Improvements of the experimental setup at low temperature will be investigated in the near future.

Acknowledgments

This work has been supported by INFN, in the Virgo R&D program, by the European Commission, in the FP6 framework (project ILIAS, research activity JR3-STREGA), and by the Italian Ministry of University and Research (MIUR-PRIN-2002).

References

[1] Braginsky V B, Mitrofanov V P and Tokmakov K V 1995 *Phys. Dokl.* **40** 564
[2] Cagnoli G, Gammaitoni L, Kovalik J, Marchesoni F and Punturo M 1999 *Phys. Lett.* A **255** 230
[3] Amico P, Bosi L, Carbone L, Gammaitoni L, Marchesoni F, Punturo M, Travasso F and Vocca H 2002 *Rev. Sci. Instrum.* **73** 3318
[4] Barr B *et al* 2002 *Class. Quantum Grav.* **19** 1655
[5] Rowan S 1999 Presentation at the *Aspen Winter Conf. on Gravitational Waves* available at http://www.ligo.caltech.edu/docs/G/G000069-00.pdf
[6] Rowan S, Byer R L, Fejer M M, Route R K, Cagnoli G, Crooks D R, Hough J, Sneddon P H and Winkler W 2003 *Proc. SPIE* A **4856** 292
[7] McGuigan D F, Lam C C, Gram R Q, Hoffman A W, Douglas D H and Gutche H W 1978 *J. Low Temp. Phys.* **30** 621
[8] Lam C C and Douglas D H 1981 *Phys. Lett.* A **85** 41
[9] Ferreirinho J 1991 *The Detection of Gravitational Waves* ed D G Blair (Cambridge: Cambridge University Press)
[10] Zener C 1938 *Phys. Rev.* **53** 90
[11] Zener C 1948 *Elasticity and Anelasticity of Metals* (Chicago, IL: University of Chicago Press)
[12] Material Properties Database (MPDB), http://www.jahm.com
[13] Swenson C A 1983 *J. Phys. Chem. Ref. Data* **12** 179
[14] Ho C Y, Powell R W and Liley P E 1972 *J. Phys. Chem. Ref. Data* **1** 279
[15] Yoon D H and Fukuda T 1994 *J. Cryst. Growth* **144** 201
[16] Chani V, Yoshikawa A, Kuwano Y, Hasegawa K and Fukuda T 1999 *J. Cryst. Growth* **204** 155
[17] Wachtman J B Jr, Tefft W E, Lam D G Jr and Apstein C S 1961 *Phys. Rev.* **122** 1754
[18] Reid S, Cagnoli G, Crooks D R M, Hough J, Murray P, Rowan S, Fejer M M, Route R and Zappe S 2005 *Phys. Lett.* A **351** 205 (*Preprint* gr-qc/0504134)
[19] Evoy S, Olkhovets A, Sekaric L, Parpia J M, Craighead H G and Carr D W 2000 *Appl. Phys. Lett.* **77** 2397
[20] Yasumura K Y, Stowe T, Chow E, Pfafman T, Kenny T, Stipe B and Rugar D 2000 *J. Microelectromech. Syst.* **9** 117